UCRL-JRNL-226405

LAWRENCE
LIVERMORE
NATIONAL
LABORATORY

Moving Dislocations in Disordered Alloys.

J. Marian, A. Caro

November 29, 2006

Physical Review B

Disclaimer

This document was prepared as an account of work sponsored by an agency of the United States Government. Neither the United States Government nor the University of California nor any of their employees, makes any warranty, express or implied, or assumes any legal liability or responsibility for the accuracy, completeness, or usefulness of any information, apparatus, product, or process disclosed, or represents that its use would not infringe privately owned rights. Reference herein to any specific commercial product, process, or service by trade name, trademark, manufacturer, or otherwise, does not necessarily constitute or imply its endorsement, recommendation, or favoring by the United States Government or the University of California. The views and opinions of authors expressed herein do not necessarily state or reflect those of the United States Government or the University of California, and shall not be used for advertising or product endorsement purposes.

Moving dislocations in disordered alloys.

J. Marian* and A. Caro

Chemistry and Materials Science Directorate,

Lawrence Livermore National Laboratory, Livermore, CA 94550

(Dated: March 14, 2006)

Abstract

Using atomistic simulations of dislocation motion in Ni and Ni-Au alloys we report a detailed study of the mobility function as a function of stress, temperature and alloy composition. We analyze the results in terms of analytic models of phonon radiation and their selection rules for phonon excitation. We find a remarkable agreement between the location of the cusps in the σ-v relation and the velocity of waves propagating in the direction of dislocation motion. We identify and characterize three regimes of dissipation whose boundaries are essentially determined by the direction of motion of the dislocation, rather than by its screw or edge character.

I. INTRODUCTION

The emergence of fully three dimensional, mesoscopic computational methodologies based on dislocation theory has given rise to several recent breakthrough observations in crystal plasticity. Calculations involving dislocation densities of the order of 10^{12} m^{-2} and higher have become accessible by using efficient computational methods such as Dislocation Dynamics (DD)[1–3]. This has provided many critical insights that are improving our understanding of strain hardening and single crystal plasticity. Dislocation multiplication giving rise to cell boundaries, dislocation forests and other collective dislocation arrangements have been simulated to high degrees of accuracy using DD[4–6]. At its core, DD is a discretized representation of dislocation lines interacting with each other via isotropic linear elasticity. This means that the rich atomistic details of the dislocation core are neglected in favor of computational efficiency. Nevertheless, given the highly non-linear character of the interatomic interactions in the core, it is clearly the relative motion of the core atoms that contributes most to the energetics of dislocation motion[7]. Therefore, no DD model is complete without a meaningful incorporation of this atomistic information. In order to understand how this can be achieved, one only needs to look at the two fundamental equations integrated during a DD simulation[8]:

$$\begin{aligned} \mathbf{v} &= \mathbf{M}\ \mathbf{f} \\ \mathbf{f} &= -\nabla_{\mathbf{r}} E_{el}\left(\mathbf{r}\right) \end{aligned} \tag{1}$$

where $\mathbf{r}$, $\mathbf{v}$ and $\mathbf{f}$ are the position, velocity, and force vectors of the set of discrete nodes representing the dislocation ensemble. E_{el} is the total elastic energy and $\mathbf{M}$ is a second-order tensor that maps the local force field at a given node onto nodal velocities. In essence, $\mathbf{M}$ maps the stress tensor of the case at hand onto the velocities for each one of the nodal degrees of freedom. The computation of the nodal velocities (mobilities) in response to the driving forces is highly material and condition specific and $\mathbf{M}$ is a complex function of many parameters including stress, temperature, dislocation character and, of course, material properties. As mentioned above, dislocation motion is intrinsically a discrete process governed by the atomic properties and discreteness of the lattice and the dislocation core. Therefore, determining the mobility law is beyond the capabilities of linear elasticity and requires more detailed, atomistic-level calculations that take into account the non-linear character of dislocation motion. Sources of this information are typically experiments, especially those performed with atomistic resolution such as HREM, or atomistic simulations. The fidelity of DD dislocations hinges heavily on these mobilities functions, whose determination is generally quite computationally exhaustive.

To date, DD simulations have been performed for pure systems in slow deformation conditions. However, there is an increasing volume of work in high-pressure physics and materials strength that imply stresses in excess of several GPa and strain rates of the order of 10^6 s^{-1} and higher as well as mixed materials such as LiF and SiO[9,10]. Under these extreme conditions, it is expected that dislocations will travel at very high velocities, possibly exceeding the speed of sound. Additionally, processes involving multicomponent systems have not yet been addressed in DD. By way of example, precipitation hardening, or age hardening, provides one of the most widely used mechanisms for the strengthening of metal alloys. In precipitate-strengthened alloys, the stress required to move dislocations appreciable distances on a slip plane is noticeably higher than in the pure matrix and thus this is the process controlling the yielding behavior of the solid. Models proposed to explain the yield strength of precipitate-strengthened materials make use of some structural features that restrict dislocation mobility, be it dislocation bowing, cross slip, particle shear, etc. These are mechanisms that are microscopic in nature and thus atomistic simulation is ideally suited to study it. Although of high technological importance, only recently have reliable multicomponent interatomic potentials been developed for the study of binary alloys. Potentials are fitted to a few well-known parameters, such as elastic properties and heats of mixing, that might not reproduce the thermodynamics satisfactorily.

In this paper, we report molecular dynamics (MD) results of edge and screw dislocation motion simulations in dilute Ni-Au alloys. In the first part of this work we discuss the continuum solutions for sub and supersonic dislocations. Subsequently, we choose the working regime within the phase diagram of the alloy based on short-range order considerations and we age the working samples to thermodynamic equilibrium. Secondly, on the previously-obtained samples, a MD study is carried out to detail the dislocation motion behavior and extract mobility laws under each corresponding regime.

II. MOVING DISLOCATIONS IN ALLOYS: THE ANALYTIC APPROACH

Dislocations moving in a crystal experience a resisitive force leading to energy dissipation. These forces originate from the intrinsic properties of the crystal, and give rise to two possible dissipation mechanisms: damping by scattering of elementary excitations existing in the lattice and radiation of waves originated by the very dislocation motion. The first mechanism can be described by a simple viscous law, with the viscosity directly proportional to the temperature, and is the dominant dissipation mechanism at low velocities. The second mechanism has a complex velocity dependence, is relevant generally at high velocities and essentially independent of temperature. Traditionally, two theoretical frameworks have been employed to study radiative dissipation, namely continuum elasticity and discrete lattice models within the harmonic approximation. However, their application to real lattices poses serious challenges when it comes to a proper quantitative interpretation. We shall focus most of this work on this problem as it still presents the biggest difficulties.

Dissipation of energy by radiation is a puzzling effect. Starting in the late 1940's with the continuum approximation, the work of Frank, Leibfried and Dietze introduced the notion of 'relativistic' motion for speeds comparable to the transverse sound velocity[11]. In the 50's, solutions based on continuum elasticity predicted dissipation-free subsonic and dissipative supersonic motion, with a divergence at c_T, the speed of transverse waves. This divergence was later characterized for screw and edge dislocations. For example, Hirth and Lothe[11] give the standard treatment of a moving dislocation in an isotropic continuum medium. It is based on the Lorentz transformations of space and time with the transverse sound velocity c_T as the limit velocity. As in relativity theory, several magnitudes diverge as v approaches c_T, in particular the self-energy of the moving dislocation and hence the stress necessary to maintain a steady motion. The concept of 'forbidden velocity' emerges from this context in which c_T appears as the maximum possible velocity. However, supersonic dislocation velocities are also possible and curious solutions (as for example dissipation-free motion at $\sqrt{2}c_T$[12]) appear in isotropic continuum elasticity above c_T.

For dispersive media, Eshelby[13] found the solution for dissipation *vs.* v at intermediate velocities. Eshelby's approximate approach in a dispersive continuum gives dissipative subsonic motion in some range above the minimum phase velocity and below c_T. This is a regime that MD simulations recently seem to have identified, although no particular relation between this minimum velocity and any relevant crystal velocity has been established[14]. In general, every additional complexity considered in the different models introduces some new characteristic velocity that appears to play a role in the mechanism of dissipative radiation.

The main conclusions extracted from c continuum analysis then are:

1. Subsonic motion is dissipation-free if the medium has no dispersion
2. As v approaches c_T from below, the singularity of the self-energy in non-dispersive media goes as:
$$\dot{W} \propto \left(1 - \left(\frac{v}{c_T}\right)^2\right)^{-\frac{1}{2}} \tag{2}$$
for screw, and as:
$$\dot{W} \propto \left(1 - \left(\frac{v}{c_T}\right)^2\right)^{-\frac{3}{2}} \tag{3}$$
for edge dislocations.
3. When dispersion is introduced but isotropy is maintained a new critical velocity appears, the slowest phase velocity $c_{min} = \omega/k$, for k in the direction of dislocation velocity. At this velocity radiation starts as:
$$\sigma \propto (v/c_{min} - 1)^{\frac{3}{2}} \tag{4}$$
for screw dislocations. The case of edge character has not been solved.

In the 70's and 80's, discrete models of even the simplest cubic lattices introduced more structure in the dissipation curve. These theoretical calculations of the relation between stress and velocity for dislocations moving in a discrete lattice were done on the basis of idealized lattice dynamics models of harmonic crystals. Celli *et al.*[15], Crowley *et al.*[16], and Ishioka[17] developed models for a screw dislocation moving in a simple cubic nearest-neighbor harmonic lattice with snapping bonds. These results were later expanded by Glass[18] to include isotopic mass defects, and the case of uniform motion was solved by Caro *et al.*[19]. Analyses of the nature of the radiation were given by Debiaggi *et al.*[20,21].

These works consider a perfect crystal at zero temperature under the influence of external Kanzaki forces as implemented by Boyer *et al.*[22]. These forces create the time dependent topology of a moving screw dislocation. In this way, the external forces act on a perfect harmonic lattice whose Green's function is known analytically and therefore the response, in particular the energy dissipation, can be easily calculated by using the fluctuation-dissipation theorem (see Caro *et al.*[19]),

$$\dot{W} = \int dk d\omega |F(k,\omega)|^2 Im G(k,\omega) \tag{5}$$

The relation between k and ω in the Kanzaki force $F(k,\omega)$, together with the dispersion relations appearing in the Green's function $G(k,\omega)$ impose selection rules for the excitation of lattice waves that give the rich behavior of the dissipation function.

Figure 1 shows the σ-v relation for a anisotropic lattice model with cubic symmetry and a ratio $c_L/c_T = 3$, where c_L is the longitudinal speed of sound along a $\langle 100 \rangle$ direction[19]. Many interesting features appear in the figure. For example, at high velocities ($v > 0.4c_L$) the motion is well defined in the sense that $\partial v/\partial\sigma > 0$, similar to continuum theory. A minimum stress, often called dynamic Peierls stress, appears at the beginning of this regime. Contrary to continuum theory solutions, the dynamic Peierls stress is non-zero and has to do with the intrinsic properties and the discreteness of the lattice. At intermediate velocities, there are regions of instability, $\partial v/\partial\sigma < 0$, and singularities, the strongest of them corresponding to a dislocation velocity equal to transverse sound velocity (in this model the two transverse branches are degenerate along the direction of dislocation motion).

These singularities are the main result of the analytic works we are reviewing here. They show the existence of many dislocation velocities with related to the phase velocity of particular phonons in the lattice for which the dissipation displays cusps. This leads to a situation where the energy radiated by the snapping bonds cannot abandon the core of the moving dislocation, thus producing divergences in the stress required to keep a steady motion. The exact nature of these singularities depends, in these models, on the artificial phonon lifetime chosen for the Green's function.

Debiaggi *et al.*[20] analyzed the spectrum of these radiated waves, finding a relation between the polarization and the Burgers vector, and between the glide plane and the direction of propagation. In particular they found that these waves are exponentially localized on the glide plane with polarization along the Burgers vector and propagation direction along that of dislocation motion. These rules, when applied to the fcc lattice of the Ni-Au system under consideration, would give us the key to locate the cusps in the σ-v relation.

It is interesting to note here that Hirth and Lothe [11] consider that there is neither experimental manifestation nor computer simulations that support the existence of these resonances. However, we should bear in mind that the sharp resonances in the model correspond to precise selection rules in a model system that does not couple motions with different polarizations, *i.e.* a simple-cubic, nearest-neighbor harmonic model, and where

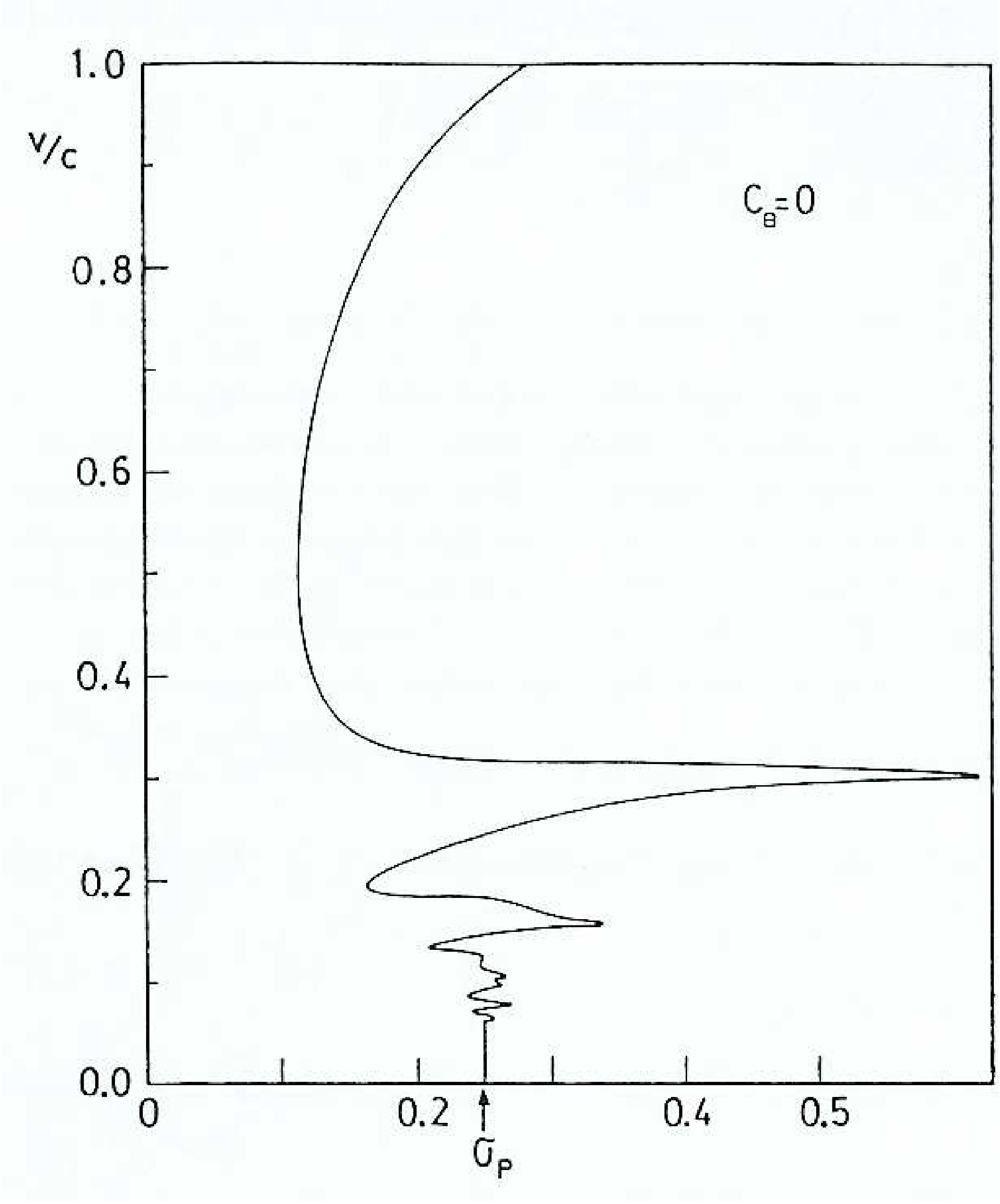

FIG. 1: Dislocation velocity normalized to longitudinal sound velocity versus applied stress normalized to shear modulus, for a screw dislocation moving in a simple cubic nearest neighbor harmonic lattice, from[19]

dislocations are ideal, radiating fully transverse polarized waves. In real crystals, as well as in computer simulations, none of these features apply, and what is observed instead of resonances is a smooth increase in radiation energy as the velocity increases. The source of this dissipation is likely to be related to both mechanisms found in the simple models explained above, namely the isotropic dispersive elastic result and the cumulus of resonances in Figure 1 for the discrete models.

The main difference between discrete and continuum models is that, in the latter, the sound velocity and the minimum phase velocity are the only two velocities that could play a role in dissipation, while in a discrete lattice the splitting between sound velocities and minimum phase velocities is a rich 3D function, as the wave vector points towards different directions in the the Brillouin zone. With this in mind, we realize that at any velocity above some absolute minimum, a dislocation is supersonic with respect to some waves and subsonic with respect to others, giving radiation of phonons at all speeds above such minimum. As a result, the fine structure of Fig 1 is lost. Finally, the analytic models also predict a rich array of dynamic effects when impurities in solid solution interact with a moving dislocation[21], which can lead to either hardening or softening of the material depending on the sign of the mass misfit. This effect on the Peierls stress does not appear when dislocations are treated in a continuum.

In summary, despite the simplified picture of dislocations and lattices given by these analytical discrete and continuum models, they have the merit of highlighting the physical nature of phonons radiated by moving dislocations, showing an unexpectedly rich behavior.

While these models represent the situation at 0K, at finite temperatures an additional mechanism of dissipation appears, namely phonon drag. This mechanism has been described, among others, by Leibfried[23] and by Brailsford[24], and gives a simple viscous damping proportional to the temperature:

$$A\,T\,\mathbf{v} = \mathbf{b}\,\sigma \tag{6}$$

A relation like Equation 6 has been found experimentally as well as observed numerous times in computer simulations.

III. MOVING DISLOCATIONS IN ALLOYS: THE COMPUTATIONAL RESULTS

It is only recently that the problem of dislocation mobility has regained some attention, as progress in computational materials science requires a proper knowledge of these functions. In a recent paper, Olmsted *et al.*[14] report atomistic simulations of dislocation mobility in Al (a fairly isotropic material), Ni (fairly anisotropic), and Al-Mg alloys, and analyze their results in terms of the forbidden velocities of the continuum models. At low velocities they find that a linear regime exists where the velocity is proportional to σ/T, as expected from phonon damping at finite temperature. They note that, in Al, screw dislocations are more damped than edge dislocations, while in Ni both behave comparably. The mobility of screw dislocations in the subsonic regime in both materials behaves as a superposition of viscous damping plus a radiative behavior with the functional form suggested by Eshelby [13], namely:

$$\sigma = \begin{cases} ATv & v < v_0 \\ ATv + D(v - v_0)^{\frac{3}{2}} & v > v_0 \end{cases} \tag{7}$$

But, despite the implications of these formulae, which suggest a crossover between a damping regime below some velocity v_0 and a radiative regime above it, they find that v_0 is not related to any relevant phonon velocity in the material, so they conclude that equations above have to be considered only as phenomenological. Furthermore, they do not provide an interpretation as to why edge dislocations do not behave in a similar way.

Other computational works that we do not discuss here address the damping regime at low velocity [25], high speed collisions with different obstacles [26], or different aspects of saturation velocities [27,28]. In general, from the collective findings of these workers, one does not get a comprehensive picture relating the structure of the mobility functions to lattice and dislocation properties.

IV. MODELING DISLOCATIONS IN Au-Ni ALLOYS

A. The Phase Diagram

For this work we have selected the Au-Ni system, described by a set of embedding-atom (EAM) potentials that are fitted to the heats of solution of the binary alloys[29], because it has recently been fully characterized thermodynamically [30]. The Au-Ni system has a simple phase diagram but unusual thermodynamic properties. The formation enthalpy is the result of the cancelation of two important terms: a positive contribution stemming from the elastic lattice distortion due to different atomic radii (r_{Au} = 1.46 Å, and r_{Ni} = 1.24 Å), that translates into a 14% lattice parameter mismatch (for Ni a_0=3.524 Å, for Au a_0=4.079 Å), and a negative chemical contribution that results from the difference in the electronegativity of the two elements. According to Lu *et al.*[31], alloys with different sign in these two contributions may show phase separation in the long range at low temperature, and short range ordering at high T. Additionally, the Ni-Au system has a large positive excess entropy derived from significant changes in the vibrational frequency spectrum when the alloy is constituted.

As shown in Ref.[30], good overall qualitative agreement with experiments is found about the main characteristics of the phase diagram. Figure 2 shows both the experimental and the calculated equilibrium phase diagrams of the Ni-Au alloy used in this work. The potentials give a narrower miscibility gap compared to the experimental measurements. There are also some manifestations of short-range order in the solid solution below saturation both experimentally and as predicted by the potentials. Therefore, Ni-Au makes for an interesting system to study dislocation mobility since one can explore regimes of ordering or segregation depending on the solute content.

B. The dispersion relation

To understand the dislocation behavior close to the forbidden velocities we focus now into the dynamic properties of the model under consideration. As discussed above, the largest cusp in the σ-v relation, see Fig. 1, appears at a dislocation velocity equal to the phase velocities of particular waves in the crystal. Phase velocities along each possible propagation direction and polarization span a range of values from a minimum, usually at the Brillouin zone edge along high symmetry directions, and a maximum close to the center of the zone, where phase (ω/k) and group ($\partial\omega/\partial k$) velocities are equal, the so-called sound velocities. Critical velocities at which singularities occur are then the slopes close to the Γ point of those phonon branches in the direction of the dislocation velocity. The red dashed lines in Figure 3 represent the minimum phase velocity, c_{min} for each k-direction. According

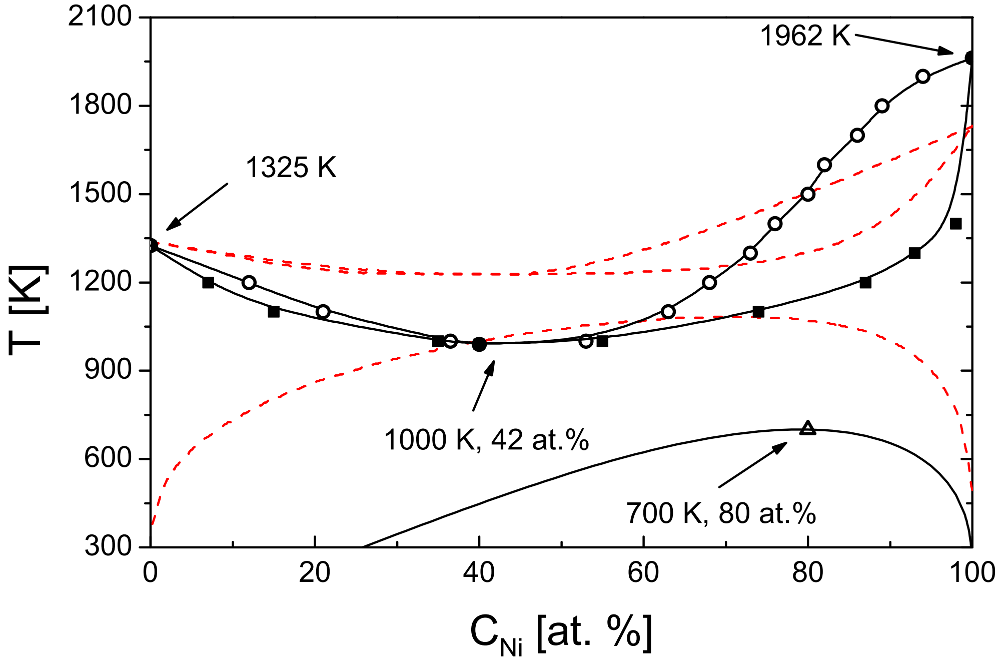

FIG. 2: Au-Ni phase diagram as obtained from the EAM potentials [29]. The experimental phase diagram (red lines) is shown for comparison, from [30]

to the arguments presented in Section II, the dissipative range of velocities for the ⟨110⟩ direction of motion, *i.e.* $c_{min} < v < c_T$, is considerably narrower than for the ⟨112⟩ direction. c_{min} for each direction are given in Table I.

Relevant wave velocities are those along the direction of dislocation motion, ⟨110⟩ for edge and ⟨211⟩ for screw dislocations. These directions correspond to the Γ-K-X and the Γ-J-X branches in Figure 3, respectively. The point that we have labeled J is not usually reported in dispersion relations; it is relevant for the process we are studying here and its location at the boundary of the first Brillouin zone is sketched in Figure 4. The sound and minimum phase velocities associated with the potential used in this work are given in Table I for the two directions of interest.

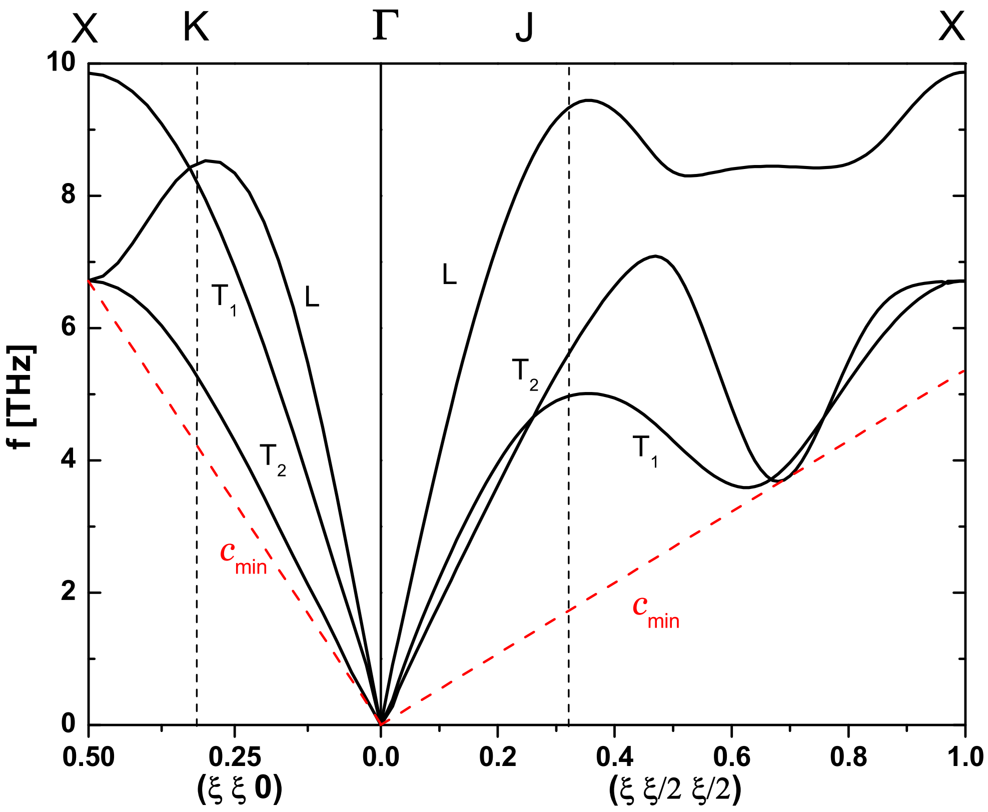

FIG. 3: Dispersion relations for pure Ni obtained with the Ni-Au EAM potential used in this work along the relevant directions dictated by dislocation motion. ξ is given in units of the reciprocal lattice parameter $4\pi/a_0$. The red dashed lines represent the minimum phase velocity, c_{min} for each k-direction. The dissipative range of velocities for the $\langle 110\rangle$ branch, *i.e.* $c_{min} < v < c_T$, is significantly narrower than for the $\langle 112\rangle$ branch.

V. RESULTS

For our molecular dynamics simulations we use a $80a \times 30b \times 40c$ (where $a = a_0\frac{\sqrt{2}}{2}$, $b = a_0\frac{\sqrt{6}}{2}$ and $c = a_0\sqrt{3}$) tetragonal sample with its principal axes oriented along $x = [110]$, $y = [1\bar{1}2]$ and $z = [\bar{1}11]$, containing 576000 atoms. Our simulated system is larger that those customarily used in similar studies, a measure aimed at minimizing finite size effects and ensuring 3D dislocation behavior. Periodic boundary conditions are used in the x and y directions, whereas traction surfaces are chosen for the z-boundaries. Perfect screw or edge dislocations with Burger vector $\frac{1}{2}[110]$ are created at the center of the sample by

TABLE I: Longitudinal, c_L, transverse, c_T, sound speeds and minimum phase velocities, c_{min}, for the two k-paths of interest: Γ-J-X for screw and Γ-K-X for edge dislocation motion. Both k-paths have non-degenerate transversal branches. The data have been calculated from the phonon dispersion relation in Figure 3. Velocities are given in m·s^{-1}.

k-branch	Γ-K-X	Γ-J-X
c_L	5637.6	5872.6
c_{T_1}	3647.3	3281.7
c_{T_2}	2132.0	2578.1
c_{min}	1927.8	766.6

applying the appropriate linear elasticity solution to the unrelaxed crystallite (screw) or by removing half planes of atoms (edge). The initial line direction is $[1\bar{1}2]$ and $[110]$ for the edge and screw dislocation respectively. Our geometry implies dislocation densities of the order of $\sim 3\times10^{15}$ m^{-2}, which can result in shear rates of 10^7 to 10^9 s^{-1}. However, results obtained in carefully carried out simulations have proven to be extrapolable to dislocations moving at the simulated velocities in materials bearing realistic dislocation densities[32]. After relaxation, both dislocations are seen to split into Shockley partials on a $(\bar{1}11)$ plane. Samples are thermally equilibrated at 100, 300 or 500 K prior to the application of the external shear stress.

With respect to the alloy systems, more details are given below. Suffice it to say that all alloys considered were aged with a Monte Carlo code [33] to build up any eventual short range order.

Shear stress is applied by imparting appropriate atomic forces on top and bottom skin regions containing one or more $(\bar{1}11)$ planes. Here we probe stresses in the $0 < \sigma < 4000$-MPa range. Dislocations start moving under the action of the applied stress and, after a transient, a steady motion develops with the dislocation crossing the sample several times depending on its speed. Linear regression fits to the dislocation position vs. time evolution provide the velocity reported in the figures below. The atoms belonging to the core of the partial dislocations and the stacking fault ribbon were identified using the centro-symmetry deviation parameter. All simulations were run using the LAMMPS code [34] with 128-256 processors on the THUNDER cluster at LLNL.

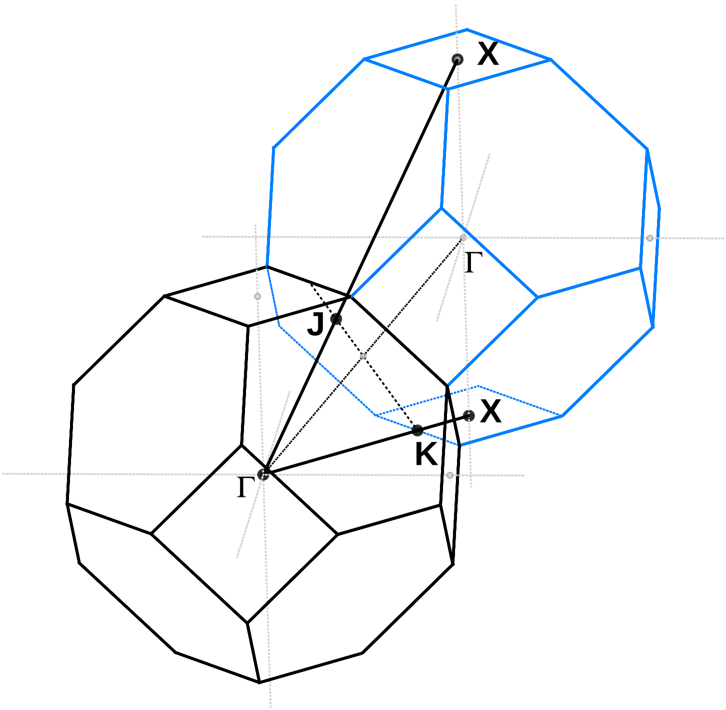

FIG. 4: Brillouin zone showing the k-branches displayed in Fig. 3 and the location of the points, Γ, K, X and J, which is the exit point of the $\langle 112\rangle$ branch from the first Brillouin zone. Note that the periodicity limits of both branches are located at point X, hence both branches come at X with equal frequency values and zero derivative.

A. Short range order vs. segregation

In choosing the alloy compositions for our study we must ensure that Au remains in solid solution in Ni at all times at the temperatures of interest. The reasons for this have to do with the possible existence of short range order, SRO, in the solid solution because of the periodic boundary conditions along the direction of motion: at every passage of the dislocation the portion of crystal above the glide plane shifts with respect to the portion below by a magnitude b; when the dislocation re-enters the box the distribution of solute atoms on the sheared section of the crystal would changed with respect to the original configuration if SRO were present. Random solid solutions do not bring about such complication. Not only this is a technical issue in the simulation setup but, if SRO develops in the solid solution, passing dislocations would alter this order producing an additional hardening effect, as discussed by Rodary *et al.* [25]. Therefore, care must be taken in ensuring that we are working in the solid solution region of the phase diagram derived from the potentials that we are using. To characterize this effect we have calculated the SRO parameter for a number of Au concentrations in Ni. The SRO is a local parameter and can be expressed as:

$$\eta_{ij} = Z_{ij} - c_j Z \tag{8}$$

where η_{ij} is the SRO parameter of species i with respect to species j, Z_{ij} is the number of neighbors of type j surrounding an atom of type i, c_j is the stoichiometric concentration of species j and Z is the total number of neighbors in the fcc lattice. In other words, the SRO parameter represents the difference between the local and global compositions. According to this definition we can contemplate the following scenarios:

$$\eta_{ij} \begin{cases} < 0 & \text{tendency to ordering} \\ = 0 & \text{random solution} \\ > 0 & \text{tendency to segregation} \end{cases} \tag{9}$$

Here we work in the range of Au concentrations for which $\eta \approx 0$. Figure 5 shows the SRO parameter as a function of Au concentration at 300K. Clearly, at $C_{\mathrm{Au}} \lesssim 20\%$ the crystal-averaged SRO exhibits no significant tendency to ordering. In contrast, at $C_{\mathrm{Au}} > 20\%$, the SRO gradually escalates indicating a strong precipitation inclination as we approach the solubility limit. Hence, in this work, we confine the dislocation mobility study to $C_{\mathrm{Au}} \leqslant 20\%$ and we choose Au concentrations of 0, 5, 10 and 20%.

B. Dislocation behavior

We now focus on mobility functions for both dislocation types at the different temperatures and Au concentrations. Unless otherwise noted, simulations were performed at increasing shear stresses until a failure mode was detected. As we shall see, for a given system size, this *maximum* stress, σ_m, strongly depends on the character of the dislocation, the simulation temperature and the Au concentration. For pure Ni it is approximately of the same order of magnitude as lower-bound estimates for the ideal shear strength of Ni (~2.4 to 7.1 GPa [35]). On the other hand, the threshold stress, σ_{th} for dislocation motion also displays the same dependences as σ_m. In pure Ni, this threshold stress is related to the Peierls stress (~6.1 MPa [36]) albeit thermal fluctuations provide a smooth extrapolation to σ_{th}=0 at least in the screw dislocation case.

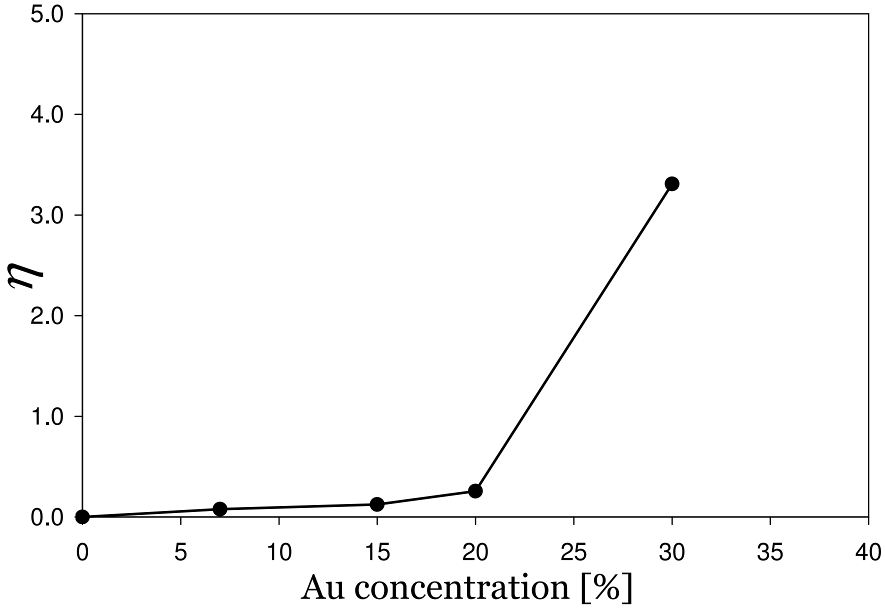

FIG. 5: Short-range order parameter for different equilibrated Ni-Au alloys at 300K. Below 20% Au content, the alloys display just traces of segregation, whereas at $C_{\mathrm{Au}} = 30\%$ the SROP grows significantly pointing to a strong precipitation tendency.

Table II contains σ_m and σ_{th} for all cases considered in this work. Interestingly, the σ_m range for screw is broader than fore edge dislocations. The only notable exception is for $C_{\mathrm{Au}} = 20\%$, for which screw dislocations do not move linearly beyond roughly 900 MPa. Conversely, σ_{th} for edge dislocations is significantly larger than for screw dislocations, a somewhat puzzling observation since, generally, the Peirls barrier for edge dislocation motion is assumed to be lower than for screw dislocations.

1. Screw dislocations

First we discuss the screw dislocation mobility along the direction of motion $\langle 112 \rangle$. Figures 6 and 7 show a family of curves representing screw dislocation velocities as a function of the applied shear stress at 100K and 300K respectively. The behavior as a function of the Au concentration is qualitative similar at both temperatures. Two dynamic regimes can readily be observed in the subsonic region. First, after overcoming the static friction (see Table II and the discussion in Section II), the dislocations start to move according to Equation 6 with friction coefficients spanning almost one order of magnitude from approximately $B = 7.8 \times 10^{-6}$ to 5.88×10^{-5} Pa·s/b at 100K as Au content increases. The friction

TABLE II: Threshold and maximum shear stresses (in MPa) for dislocation motion for all cases simulated.

Dislocation type	screw				edge			
Au %	0.0	5.0	10.0	20.0	0.0	5.0	10.0	20.0
T	100K							
σ_{th}	0	80	100	150	125	125	175	190
σ_m	3000	2600	2100	900	2600	2000	2200	1800
T	300K							
σ_{th}	0	60	100	125	100	175	175	200
σ_m	3000	2400	2100	500	2400	2200	2200	1800

coefficients $B = AT$ and A in Equation 7 are given in Table III. Theoretically, assuming ideal phonon damping in the first linear regime, the magnitude A should be independent of temperature, a criterion that our simulations generally meet (more details are given in Section 11 and Figure 11 below).

Secondly, the mobility curves experience a marked transition and level off into a more damped dynamic regime. This transition takes at a critical velocity, v_0, which is directly correlated with the value for c_{min} in Figure 3 (given in Table I) and displays a strong composition dependence. It also should mark the change from phonon drag to radiative damping as the dominant dissipative mechanism during dislocation motion. In fact, following Eshelby[13] and Olmsted *et al.*[14], we fit our data to the power law $\sigma = D\left(v - v_0\right)^{\alpha}$, where v_0 plays the role in the real crystal of c_{min} in the simplified continuum analysis (see Equation 4). The values for the critical velocities, v_0, and exponents, α and for the proportionality constant,D, are given in Table III. The curves for 20% Au did not possess sufficient structure for this kind of numerical analysis and no fits were performed.

Generally, D is seen to increase with temperature and Au content, except an anomalous data point at 300K and $C_{\mathrm{Au}} = 10\%$. The power law exponents range, approximately, between 0.65 and unity, with a clearly decreasing trend being observed as a function of C_{Au} and T. Ostensibly, the critical velocities show no temperature dependence, decrease with Au composition and are about twice the value of c_{min} along the $\langle 112 \rangle$ direction (see Table I). In any event, the second regime continues until the velocity saturates at a value

TABLE III: Friction coefficients, critical velocities and radiative exponents for the screw dislocation $v - \sigma$ dependence during the first and second dynamic regimes observed in the mobility functions.

Au %	0.0	5.0	10.0	20.0
T [K]	100			
B [$\times 10^{-5}$Pa·s/b]	0.78	1.18	2.85	5.88
A [$\times 10^{-7}$Pa·s·K^{-1}/b]	0.78	1.18	2.85	5.88
v_0 [m·s^{-1}]	1640	1500	1371	–
D [10^6 Pa·s·m^{-1}]	3.89	13.65	32.13	–
α	0.99	0.78	0.75	–
T [K]	300			
B [$\times 10^{-5}$Pa·s/b]	2.03	2.76	2.83	6.93
A [$\times 10^{-7}$Pa·s·K^{-1}/b]	0.68	0.92	0.94	2.31
v_0 [m·s^{-1}]	1639	1498	1385	–
D [10^6 Pa·s·m^{-1}]	20.93	35.76	22.78	–
α	0.71	0.63	0.70	–

of approximately 2550 m·s^{-1} for pure Ni at both 100 and 300K. However, at 5% Au this saturation is only partially identifiable, whereas at 10 and 20% at. Au the crystal becomes mechanically unstable well before this saturation velocity is reached. For pure Ni, this velocity coincides with the lower shear wave velocity in the direction of dislocation motion, $c_{T_1} = 2578$ m·s^{-1}, also plotted in Figures 6 and 7 for reference. At both temperatures, the stress required to leap into the transonic regime is approximately 2600 MPa, after which the continuity of the mobility curve is broken and the dislocation is seen to trespass this first transonic barrier very abruptly. Thus, this singular behavior represents a third identifiable dynamic regime, the singular regime.

The interpretation for this behavior can be found by identifying this transonic leap with the cusps shown in Figure 1. In this instance, the energy dissipated by the slipped atoms cannot escape the dislocation core and an infinite stress is required in order to keep the dislocation moving. At still higher stresses the system becomes mechanically unstable, an effect related to the high strain rate that results from finite size effects.

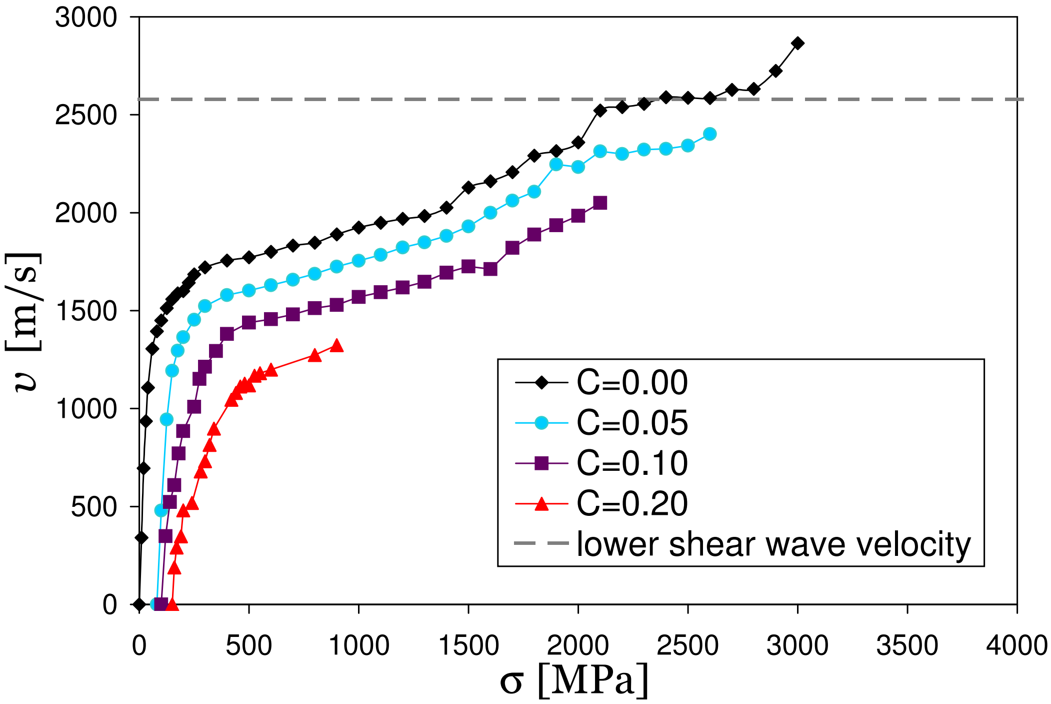

FIG. 6: Mobility at 100K for a screw dislocation moving in a Ni crystal with varying Au concentration. Two dynamic regimes can be clearly observed corresponding to two different dissipation mechanisms. For pure Ni, the dislocation velocity saturates at $c_{\langle 112\rangle}$, after which a marked leap into the transonic regime is observed.

2. Edge dislocations

We now analyze the dynamic behavior of edge dislocations. In this case, as mentioned above, the propagation direction is $\langle 110\rangle$. Figures 8 and 9 show the mobility curves at 100 and 300K respectively. The behavior of the edge dislocations is substantially different to the screw dislocations. Initially, the edge dislocation velocity grows linearly with stress until it levels off and saturates for pure Ni at a value of $c_{T_2} = 2132$ m·s^{-1}, *i.e.* the maximum value of the lower shear wave speed along the $\langle 110\rangle$ direction. Phonon drag is the main dissipative mechanism up to a critical velocity v_0, ver close to c_{T_2}, when the dislocation is seen to enter the singular regime after displaying, apparently, no radiative behavior. The critical velocities at which the dislocations transition from the phonon damping regime into this singular behavior vary with $C_{\rm Au}$, and are given in Table IV. One can see immediately that, especially at 300K, the gap between the measured v_0's and c_{T_2} for the $\langle 110\rangle$ direction

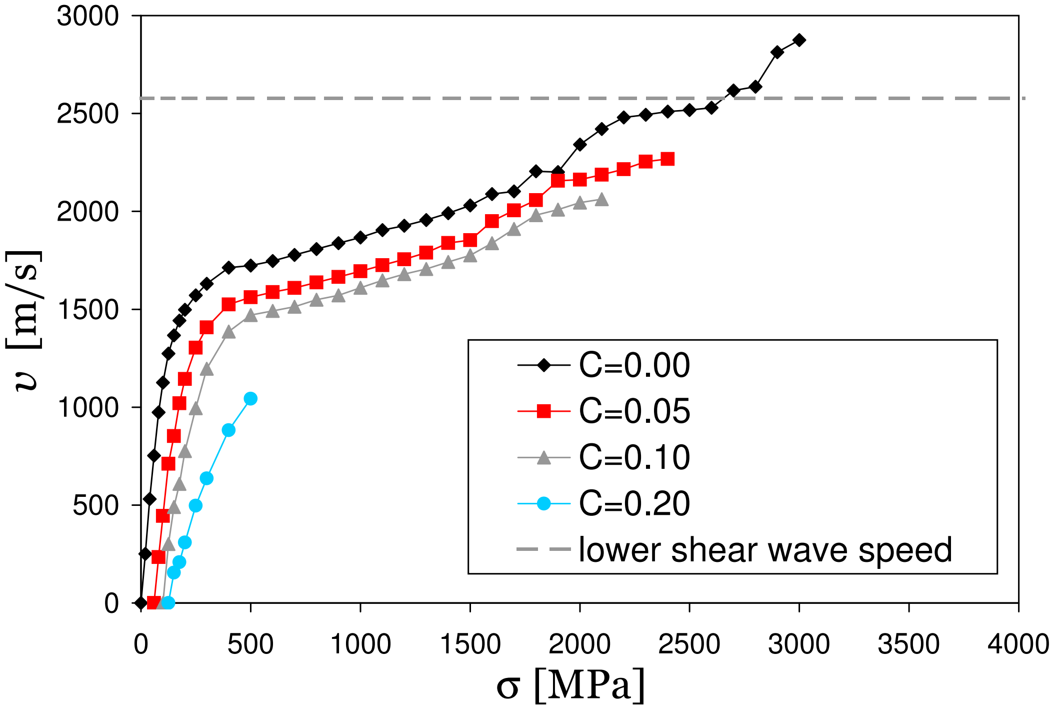

FIG. 7: Mobility at 300K for a screw dislocation moving in a Ni crystal with varying Au concentration. Similar to the 100K case, two dynamic regimes can be observed. For pure Ni, the dislocation velocity saturates at $c_{\langle 112 \rangle}$, after which a marked leap into the transonic regime is observed.

(2132 m·s^{-1}) is significantly lower than for the screw dislocation case.

At $C_{\mathrm{Au}} = 20\%$ the mobility curves lose most of the structure observed at lower Au contents and the transition from the phonon damping regime to the singular behavior becomes difficult to distinguish, albeit the transonic transition can still be appreciated. Table IV contains the friction coefficients and critical velocities as a function of Au content and temperature.

The most striking difference with respect to the screw dislocation behavior is that the transonic stress for edge dislocations is about 1050 MPa for both temperatures simulated irrespective of the Au concentration. Subsequently, for a range of velocities $c_{T_2} < v < c_{T_1}$ the dislocation enters the transonic regime, and presumably undergoes radiative damping of the form given by Eq. 7 followed by a singular behavior close to the upper shear wave velocity $c_{T_1} = 3647$ m·s^{-1}. At a stress of about 2.5 GPa (at both 100 and 300K), the dislocation in pure Ni is seen to break c_{T_1} into another regime. Only the pure system is mechanically able to withstand such elevated stresses but all the other alloys show the same qualitative

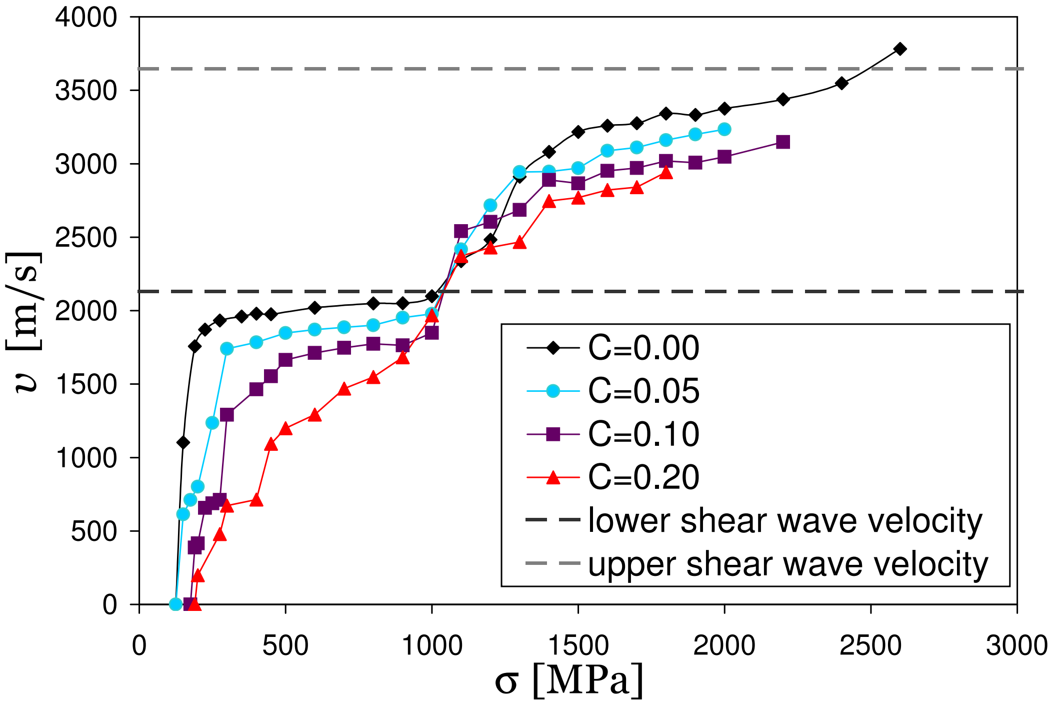

FIG. 8: Mobility at 100K for an edge dislocation moving in a Ni crystal with varying Au concentration. In this case, the dislocation moves in the phonon drag regime until it asymptotically reaches the lower shear wave velocity. Then it trespasses the transonic limit, seemingly behaving singularly again until the velocity saturates at the upper shear wave velocity. Only the pure Ni system is able to withstand the strain rates necessary to leap into the second transonic stage.

behavior, with their velocities saturating just below their effective forbidden velocity, see Table IV.

At these elevated velocities, $v > c_{T_2}$, most of the edge dislocations are seen to develop twinning partials leading to loss of mechanical stability.

VI. DISCUSSION

Figures 6 to 9 clearly suggest that dislocation motion is a complex phenomenon. Indeed, attempts to understand its intricacies span more than 50 years of research and focus onto several aspects, such as the Peierls stress, alloy composition, and the sources of dissipation, phonon drag and radiation. In what follows we analyze each aspect separately.

TABLE IV: Friction coefficients and critical velocities for the edge dislocation v-σ dependence observed in the mobility functions.

Au %	0.0	5.0	10.0	20.0
T [K]	100			
B [$\times 10^{-5}$Pa·s/b]	0.57	2.54	2.70	6.69
A [$\times 10^{-7}$Pa·s·K^{-1}/b]	0.57	2.54	2.70	6.69
v_0 [m·s^{-1}]	1103	1235	1291	1200
T [K]	300			
B [$\times 10^{-5}$Pa·s/b]	2.05	3.26	5.07	6.76
A [$\times 10^{-7}$Pa·s·K^{-1}/b]	0.68	1.09	1.69	2.25
v_0 [m·s^{-1}]	1784	1597	1571	1148

A. Critical velocities

Polarization effects give rise to two possible scenarios, depending on whether the mobility is governed by the overall behavior of the perfect dislocation or by the individual behaviors of the Shockley partials into which the perfect dislocation splits. It is worth mentioning here that the analytic calculation in [19] was done for a case where no partials exist, so this additional complexity was not treated there.

If the Burgers vectors of the partial dislocations, namely $b = \frac{1}{6}\langle 121\rangle$, are the ones that dictate the mobility behavior, then the radiated waves will be the result of the superposition of longitudinal and transverse modes for both branches. If, on the contrary, the relevant Burgers vector is that of the perfect dislocation, $b = \frac{1}{2}\langle 110\rangle$, then waves will have pure longitudinal or pure transversal polarizations for the edge and screw dislocations respectively. Comparing with the numerical results reported above, one gets the impression that in more realistic models like molecular dynamics, none of these scenarios apply. For screws, the perfect Burgers vector is orthogonal to the velocity vector, whereas partials have both normal and parallel components. Therefore, as observed in Figures 6 and 7, the singularity appears at the lowest transverse sound speed, and we may conclude that the polarization of the perfect dislocation is the one that matters. In the case of edge dislocations, the perfect Burgers vector is longitudinal with respect to the direction of motion, and the partials also

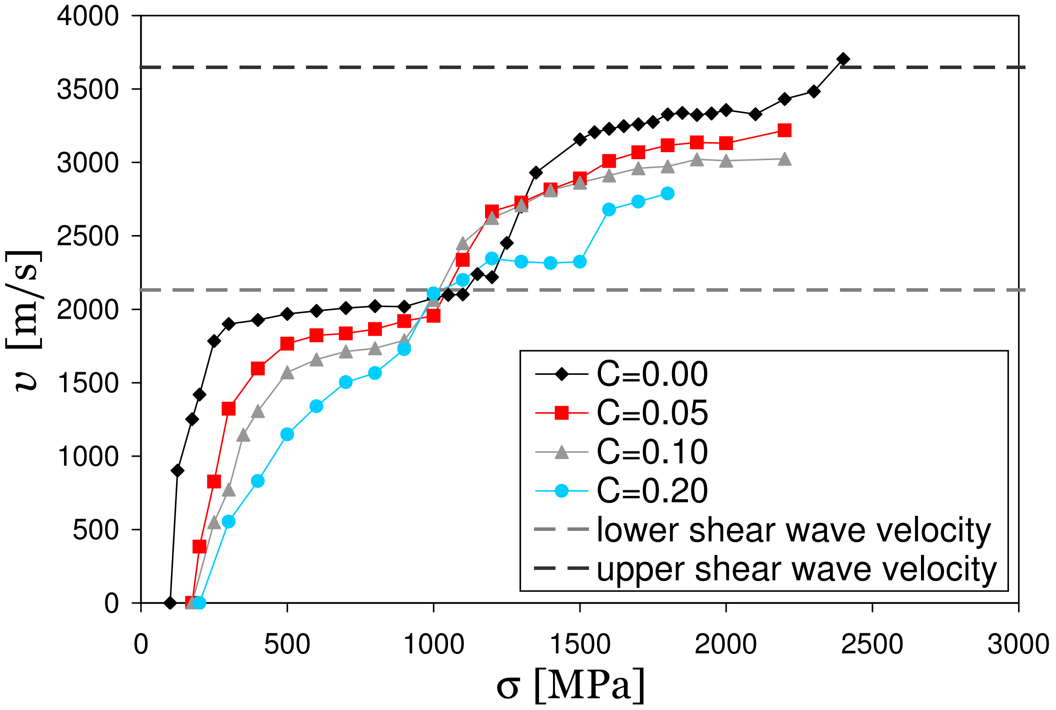

FIG. 9: Mobility at 300K for an edge dislocation moving in a Ni crystal with varying Au concentration.

have mixed components. However, as shown in Figures 8 and 9, the singularity also appears at the two transverse sound speeds, so we cannot conclude which polarization is dominant.

Thus the only interpretation that satisfies the whole ensemble of observations is that both polarizations are relevant, and that all sound speeds, regardless of their polarization, introduce singularities. In our model displacements are coupled and thus dislocations do not emmit waves with a well defined polarization. We conclude that our simulations do not show singularities at longitudinal modes simply because such high velocities were not reachable in our system due to finite size effects, but we speculate that using larger samples the entire transonic and supersonic regimes could be mapped and singularities should be observed also at c_L.

With regard to the difference between the sequence drag→radiation→singularity observed for screws, and drag→singularity observed for edge dislocations, we conclude that the reason is to be found in the difference between minimum and maximum phase velocity along Γ-J and Γ-K branches, see Figure 3. The radiation regime appears in a window between c_{min} and c_{T_2}; for edge dislocations c_{min} is very close to c_{T_2} and therefore the radiation regime is overrun by the singularity regime. Instead, in screw dislocations c_{min} is approximately half the value of c_{T_2} and there is therefore a wide v-range where this regime is dominant.

Therefore, from the MD simulation results and the simple models discussed above, we can conclude the following:

- There is a minimum velocity ($\sim 0.1c_T$ in Fig 1 and $\sim 0.3c_T$ in our MD simulations), below which radiation is suppressed and only phonon drag is significant. This minimum velocity is related to c_{min}, defined in Figure 3.
- Supersonic motion is clearly possible and beyond c_T analytic calculations suggest that the v-σ relation is smooth, although this regime cannot be reached in our MD simulations due to finite size effects that lead to mechanical failure of the computational cell. Moreover, we have demonstrated that dislocations can be accelerated beyond transonic barriers, in disagreement with some works published in the literature[27,37].
- Screw and edge dislocations behave differently. While edge dislocations go from a regime of viscous damping (phonon drag) to a regime dominated by singularities, screws show an additional intermediate regime of radiative dissipation. We speculate that this regime is the equivalent in real crystals to the multi-singularity regime observed below c_T in the simple discrete analytical model discussed in Section II (see Figure 1) and in the continuum model of Eshelby [13] with a single singularity at c_T. Figures 6 and 7 strongly suggest such relationship, although it has to be noted that the exponent is different. We capture the complex behavior of the superposition of several weak singularities into a functional form similar to the case of a single singularity, but where the exponent and the velocity c_{min} are not related in a simple way to the dispersion relation of the material. We interpret the difference between screw and edge in terms of the small window of possible velocities up to c_{T_2} in the direction of motion of the edge dislocations. The singularity at c_{T_2} hides, we believe, the intermediate regime. With this interpretation a single mobility law can be formulated for both dislocation types.
- There is an unequivocal relation between the singularities and the velocity of transverse polarized waves traveling in the direction of the dislocation motion, as determined from the phonon dispersion relations. However, there is no direct connection between the

direction of the Burgers vector of either the partials or the perfect dislocations and the branches in the dispersion relations as it happens in the idealized harmonic model [19].

- For edge dislocations there is a peculiar v-σ pair, namely $v = c_{T_1} \simeq 2100$ m·s^{-1} and $\sigma \simeq 1100$ MPa where all curves meet, regardless of temperature and composition, *i. e.* all alloys at all temperatures studied cross the first singularity at the same stress level. The reason for the existence of this point remains unclear, as from the analytic approach, the strength of the singularity depends on the phonon life time, i. e. anharmonicities of the lattice, and by changing composition and temperature, this property certainly changes. We believe this feature may be related to size effects.

B. Temperature dependence

For the temperature analysis, we confine the discussion to the results in pure Ni to separate this from composition effects that will be discussed below. Phonon drag, relevant at low dislocation speeds and moderate to high T has been successfully characterized by several workers[23,24] and its effect is well captured by a viscous term that depends linearly on T, $B = AT$. As discussed earlier, here A is the temperature-independent viscosity and should remain constant in the dynamic regime where phonon drag is dominant. We have performed additional simulations to further substantiate this and the results are shown in Figure 10. The figure shows the mobility of screw dislocations in pure Ni at three different temperatures, namely 100 and 300K, already discussed in Section V B 1, and also 500K. The data for A at 100 and 300K was already presented in Table III, 7.82×10^{-8} and 6.77×10^{-8} Pa·s·K^{-1} per unit Burgers vector respectively, and to this we add a value of $A = 6.624 \times 10^{-8}$ at 500K in the same units. Therefore, our simulations capture the dynamic behavior of the phonon drag regime quite accurately and are in excellent agreement with the data obtained by Olmsted *et al.*[14] for screw dislocation simulations in Ni using MD.

Another striking feature in Figure 10 is that, after the initial viscous regime, the dynamical behavior of the screw dislocations becomes temperature independent. The transition into the radiative regime scales almost linearly with temperature ($\sigma/T \sim 0.3$ for all three temperatures) but, once established, this radiative dissipation is characterized by a law of the type $\sigma \propto v^{\alpha}$, with α being close to unity. More details are given in Section VI D concerning

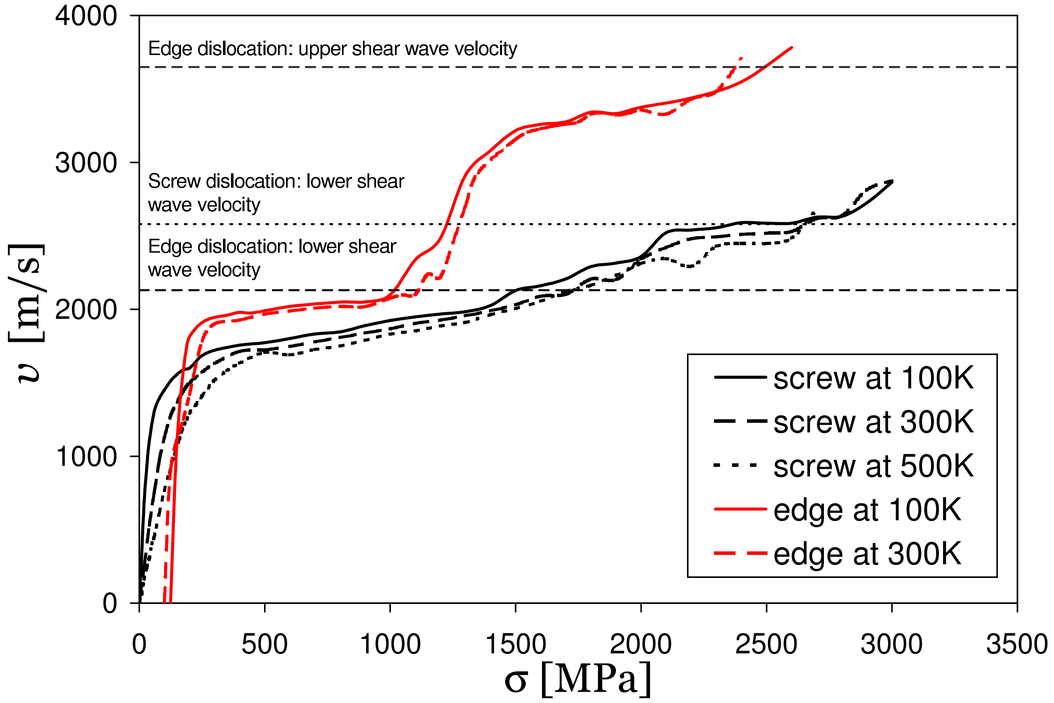

FIG. 10: Dislocation mobility in pure Ni as a function of temperature. For screw dislocations, the figure showcases the three dynamic regimes studied in this work: phonon drag, radiative dissipation and singular regimes. For edge dislocations, the radiative region is suppressed on account of the narrow gap between v_0 and c_{T_1} for the direction of motion (see text). The data at 100 and 300K were already presented in Figures 6 and 7 for screws and 8 and 9 for edge dislocations.

the functional form of the σ vs v dependence in this regime..

Similarly, as the dislocation approaches the lower shear wave speed, the three cases display the same qualitative behavior. At 500K the σ-v curve loses some resolution due to thermal noise, although the transonic stress is the same as for 100 and 300K and equal to 2700 MPa.

With regard to edge dislocations, similar conclusions can be extracted. The values for A at 100 and 300K for pure Ni are given in Table IV and are 0.57×10^{-7} and 0.68×10^{-7} Pa·s·K^{-1} per unit Burgers vector respectively, again in good agreement with Olmsted *et al.*. Evidently, two data points are not enough to derive a conclusive trend but the respective values are within a tolerable margin and seem to validate the expected dynamic behavior in the phonon drag regime.

In stark contrast with screw dislocations, here the mobility curve transitions into a temperature-independent, singular behavior leaving no indication of the development of a radiative regime. As mentioned in Section VI A we conclude that this is caused by the narrow range of available wave velocities between the minimum phase velocity and the sound velocity along the $\langle 110 \rangle$ direction (see Figure 3) when compared to the $\langle 112 \rangle$ direction, pertinent to screw dislocations. In other words, $(c_T - c_{min})_{\text{edge}} \ll (c_T - c_{min})_{\text{screw}}$. As pointed out in Section V B 2 and shown in Figure 10, the first transonic stress is around 1000 MPa and is also temperature (and composition) independent. The subsequent singular behavior, in the transonic regime, also bears no temperature dependence, nor does the second transonic stress (at about 2400 MPa).

In conclusion, in pure Ni, temperature is only a factor to consider when dislocations operate within the phonon drag regime at low velocities. The dependece follows Equation 6 very accurately and the corresponding viscosities are given in Tables III and IV. In the other two regimes, both types of dislocations exhibit a temperature-independent behavior.

C. Composition dependence

The alloying effects manifest themselves mainly through two features, namely the threshold stresses and the viscous damping coefficients. The threshold stresses, σ_{th}, are given in Table II for all cases simulated in this work. Several theories have been proposed over the last decades to explain the origin of σ_{th}. These theories have mostly been formulated on the basis of direct dislocation-solute interactions (see Ref.[38] and references therein) or solute-solute associations induced by dislocation glide[25,39]. Other non-elastic mechanisms such as electrostatic locking[40] have also been proposed, but they will not be considered here as are not captured by our potentials.

Contrary to the Ni-Al system studied by Rodary *et al.*[25], where there is a strong tendency to ordering and therefore, in principle, Al-Al pairs repel, Au in dilute solution in Ni exhibits a weak inclination to segregation (see Figure 5). This means that the mechanism responsible for chemical hardening cannot be explained in terms of an increase of repulsive solute dimers across the glide plane. In our case, solute hardening appears as a consequence of elastic interactions between dilatational inclusions (the Au atoms) and the volumetric stress field of the dislocation. The interaction is thus “dielastic” in the sense of Kröner, *i.e.* it is induced by the dislocation[41]. Another factor to take into account is that, although a perfect screw dislocation possesses no volumetric stress component, its intrinsic dissociation into a pair of Shockley partials in fcc materials projects the total Burgers vector into an edge and a screw component. Nevertheless, the edge component of the partials resulting from a perfect screw is only $1/\sqrt{3} \sim 0.57$ times that of a perfect edge. At this point we make two interesting considerations. First, since it is only the edge component that interacts elastically with the solute atoms, one would expect σ_{th} to be some function of the edge component of the Burgers vector. Secondly, the intrinsic lattice barrier to dislocation motion in a material (the so-called Peierls barrier in a pure system) is known to scale linearly with b. As anticipated in Section V B, the threshold stress in dilute alloys is directly related to this intrinsic barrier in the pure material. Therefore, following this line of reasoning, the threshold stress for screws should be approximately 0.57 times that for edge dislocations. Notably, the ratios taken from Table II at 100K are in very good agreement with this estimate: ${\sigma_{th}}_{\text{screw}}/{\sigma_{th}}_{\text{edge}} =$ 0.64, 0.57 and 0.78 for 5, 10 and 20% Au respectively.

With regard to the friction coefficients given in Tables III and IV, there are several important observations. First, the presence of solute atoms introduces an additional temperature dependence for A in the phonon drag regime. Figure 11 shows the four coefficients of the phonon drag regime versus composition. We see that the T dependence of A with Au content is well described by an expression such as: $A(T, x) = A^* + x\beta(T)$, where A^* is the temperature independent value of $A(T, 0)$, x is the Au content and $\beta(T)$ is the slope of the curves shown in Figure 11. Then, at low velocities, our results agree well with those of standard hardening models[42] in that phonon drag coefficient is proportional to the solute concentration. Secondly, for screw dislocations (Figures 6 and 7), during the radiative and singular regimes there is no appreciable composition dependence, the curves run qualitatively in a similar fashion scaled by an attenuation factor inherited from the phonon drag regime. A similar argument can be made for the singular regimes observed during edge and screw dislocation motion.

Hence, we conclude that the origin of the static threshold stress calculated in our simulations lies in the local elastic interaction between the dislocations and the solute Au atoms, and its strength is dictated by the edge character of the partial dislocations. On the other hand, the system's chemical composition does not overly affect the temperature-independent behavior at low velocities. At a fixed temperature, a proportionality is found between A and the Au content. No dislocation-specific behavior is observed.

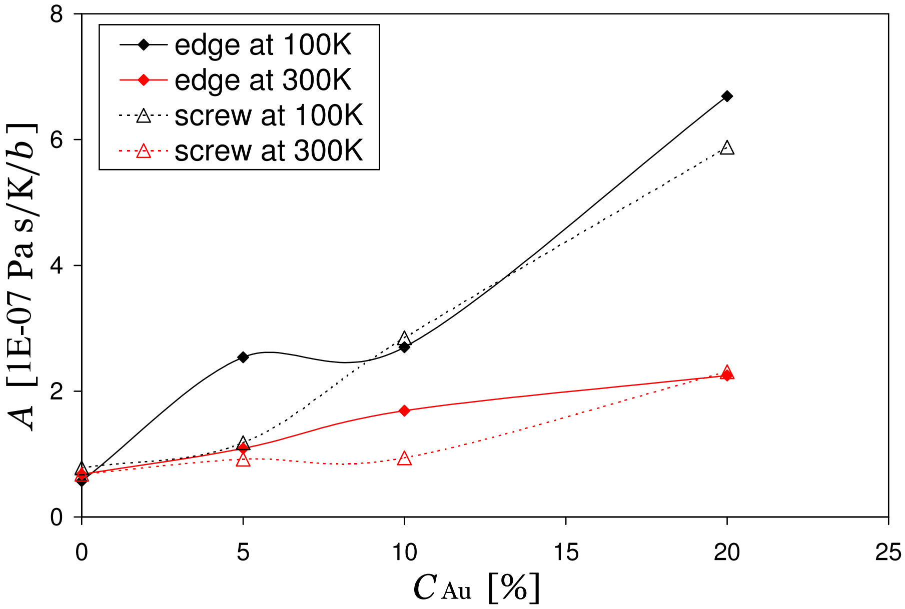

FIG. 11: Temperature-independent friction coefficient A for screw and edge dislocations as a function of composition. Generally, equal temperatures correlate together except most notably at 5% Au at 100K. The lines connecting the datapoints are just a guide to the eye.

D. Mobility functions

To summarize our observations, we present here the general form of the mobility law, taking into consideration all three regimes observed in our simulations and the theoretical framework used to interpret them. As we have seen, there are three types of contributions to the dynamic dissipation:

- A phonon drag term that holds at all velocities, characterized by a viscosity that depends linearly on all three magnitudes explored, namely temperature, the magnitude of Burgers vector and, to first order, Au content.

- A radiative term that holds only at velocities above the minimum critical velocity c_{min} related to the minimum phase velocity along the direction of motion of the dislocation. This term is expressed by a power of the difference between the dislocation velocity and the minimum phase velocity, with an exponent in the range $\frac{1}{2}$ to 1 that displays little or no dependence on composition.

- Several (up to three) singular terms at the maximum phase velocities, *i. e.* the sound velocities c_{T_1}, c_{T_2} and c_L, which do depend, albeit weakly, on the alloy composition.

> Every singularity holds up to a maximum stress, at which the $v - \sigma$ curve presents a discontinuity. The critical exponents depend on dislocation type, and are also in the range $\frac{1}{2}$ to $\frac{3}{2}$. Our results do not provide enough information to relate these stress values to any of the parameters explored. Moreover, while intuitively these values should be related to anharmonicities, the effects of solutes is not apparent.

The combination of these terms gives the following functional form for the mobility law::

$$\begin{aligned} \sigma &= \left(A^* + x\beta(T)\right) Tbv + D\,(v - v_0)^\alpha\,\theta(v - v_0) + \\ &+ \sum C_i(x)\,(c_{T_i} - v)^{-\beta_i}\,\theta(c_{T_i} - v) \end{aligned} \tag{10}$$

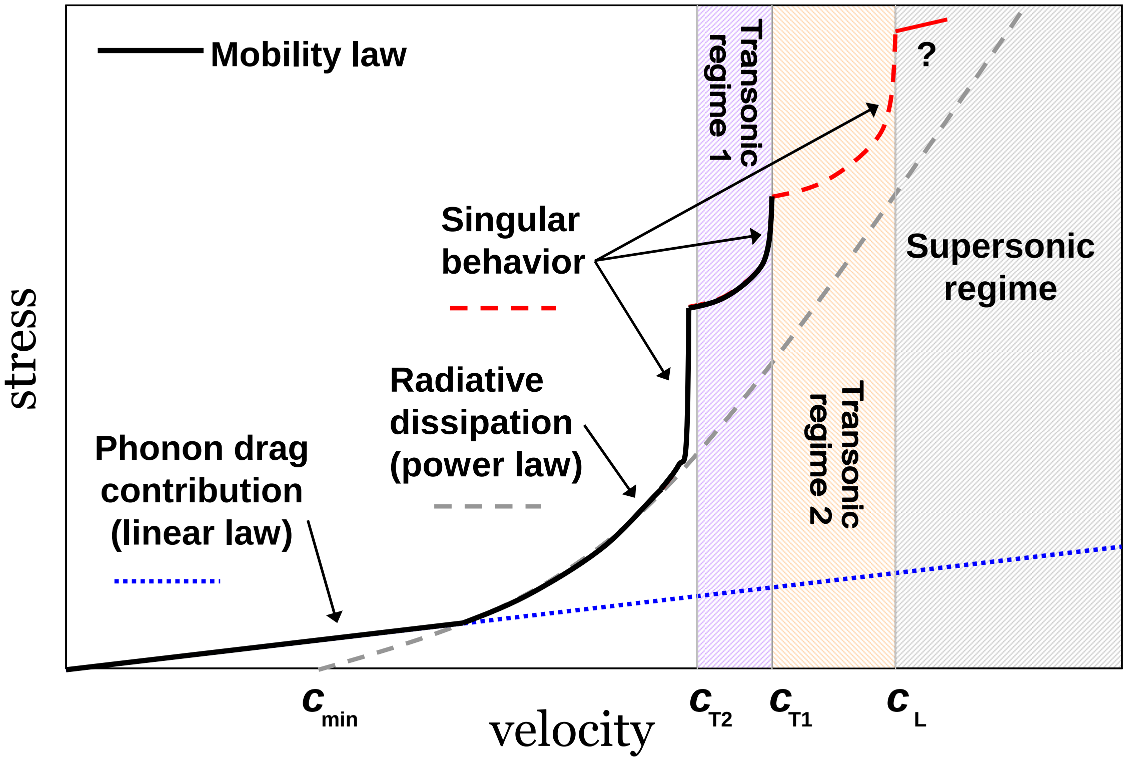
Mobility law
Transonic regime 1
?
Singular behavior
Supersonic regime
Radiative dissipation (power law)
Transonic regime 2
Phonon drag contribution (linear law)
stress
$c_{\min}$
velocity
c_{T2}
c_{T1}
c_L

FIG. 12: Schematic plot of the three dynamic regimes observed in our simulations. Each regime corresponds to a term in Equation 10. The enveloping black curve is the range observed in this work.

A schematic representation of this function is given in Figure 12. Finally, for every material and every direction of motion, the dispersion relations give the values for minimum and singular velocities.

VII. CONCLUSIONS

We have studied the relation between applied stress and dislocation velocity in a model alloy using computer simulations. The obtained mobility curves display a rich structure, expressed in the form of an intricate functional form, which we interpret resorting to continuum and discrete models of dislocation dynamics.

We prove that dislocation motion is a superposition of three different dynamic regimes punctuated by critical velocities. We have established relations between the phonon spectrum of the lattice and the structure of the mobility function. These relations remove long-standing uncertainties found in the literature concerning the interpretation of these critical velocities, as we show that they are clearly related to the phase velocities of phonons propagating in the direction of dislocation motion.

Our main conclusion, thus, is that our MD simulations satisfy the velocity selection rules derived from the continuum and discrete lattice dynamics analysis. Our simulations confirm the validity of the phonon damping mechanism as being linear with temperature and independent of dislocation character. Additionally, our data suggest that the threshold stress for dislocation motion depends linearly with the alloy composition, resulting from elastic interactions among solute atoms and the hydrostatic component of the stress field of the moving dislocation.

Finally, we are led to conclude that, seemingly, the direction of motion is the overarching parameter governing dislocation dynamics, rather than its character. In our model system and in the stress and temperature ranges explored, we find no indication that dislocation character plays any significant role in the dynamic properties of the moving dislocations. Nevertheless, one needs to bear in mind that our data have been obtained under very specific conditions. To name but a few: the crystal structure considered is fcc and, hence, our conclusions are circumscribed to this type of materials; the stress state is simple shear so that there are only glide forces acting upon the dislocations. These are not necessarily limitations but simply final cautionary remarks to put our conclusions into perspective. More simulations broadening the parametric space explored here are needed in order to consolidate our observations.

Acknowledgments

Work performed under the auspices of the U.S. Department of Energy by the University of California Lawrence Livermore National Laboratory under contract No. W-7405-ENG-48 and the Laboratory-directed Research and Development Office under program 06-ERD-005.

---

[*] Electronic address: `marian1@llnl.gov`

[1] H. M. Zbib, T. D. de la Rubia, M. Rhee, and J. P. Hirth, J. Nucl. Mater. **276**, 154 (2000).

[2] V. V. Bulatov, M. J. Tang, and H. M. Zbib, MRS Bulletin **26**, 191 (2001).

[3] V. V. Bulatov, J. Comp.-Aided Mat. Des. **9**, 133 (2002).

[4] C. Depres, M. Fivel, C. Robertson, A. Fissolo, and M. Verdier, J. Physique IV **106**, 81 (2003).

[5] A. Arsenlis and M. Tang, Modelling Simul. Mater. Sci. Eng. **11**, 251 (2003).

[6] M. Hiratani and V. V. Bulatov, Philos. Mag. Let. **84**, 461 (2004).

[7] W. Cai, *Handbook of Materials Modeling* (Springer, S. Yip (Ed.), 2005).

[8] W. Cai and V. V. Bulatov, Mater Sci Eng A **387-389**, 277 (2004).

[9] N. C. Woolsey and J. S. Wark, J. Appl. Phys. **81**, 3023 (1997).

[10] D. G. H. *et al.*, Phys. Plasmas **12**, 082702 (2005).

[11] J. P. Hirth and J. Lothe, *Theory of Dislocations* (Krieger Publishing Company, Malabar, Florida, 1992).

[12] J. D. Eshelby, Proc. Phys. Soc London A **62**, 307 (1949).

[13] F. D. Eshelby, Proc. Phys. Soc. London B **10**, 1013 (1956).

[14] D. L. Olmsted, L. G. H. Jr, W. A. Curtin, and R. J. Clifton, Modelling Simul. Mater. Sci. Eng. **13**, 371 (2005).

[15] V. Celli and N. Flitzanis, J. Appl. Phys. **41**, 4443 (1970).

[16] S. Crowley, N. Flytzanis, and V. Celli, J. Phys. Chem. Solids **41**, 63 (1980).

[17] S. Ishioka, J. Phys. Soc. Japan **34**, 462 (1973).

[18] N. Glass, J. Physique **44**, 741 (1983).

[19] A. Caro and N. Glass, J. Physique **45**, 1337 (1984).

[20] S. R. de Debiaggi and A. Caro, J. Physique **48**, 1499 (1987).

[21] S. R. de Debiaggi and A. Caro, J. Physique **48**, C8/359 (1987).

[22] L. L. Boyer and J. R. Hardy, Philos. Mag. **24**, 647 (1971).

[23] G. Liebfried, Z. Phys **127**, 344 (1950).

[24] A. D. Brailsford, J. Appl. Phys. **43**, 1380 (1972).

[25] E. Rodary, D. Rodney, L. Proville, Y. Brchet, and G. Martin, Phys. Rev. B **70**, 054111 (2004).

[26] C. Woo, Mater Sci Eng A **350**, 223 (2002).

[27] P. Gumbsch and H. Gao, Science **283**, 985 (1999).

[28] P. Rosakis, Phys. Rev. Lett. **86**, 95 (2001).

[29] S. M. Foiles, M. I. Baskes, and M. S. Daw, Phys. Rev. B **33**, 7983 (1986).

[30] E. O. Arregui, M. Caro, and A. Caro, Phys. Rev. B **66**, 054201 (2002).

[31] Z. W. Lu and A. Zunger, Phys. Rev. B **50**, 6626 (1994).

[32] J. Marian, W. Cai, and V. V. Bulatov, Nature Materials **3**, 158 (2004).

[33] B. Sadigh and *et al.*, to be published (2005).

[34] S. J. Plimpton, J Comp Phys **117**, 1 (1995).

[35] M. Yamaguchi, M. Shiga, and H. Kaburaki, Science **307**, 393 (2005).

[36] P. Szelestey, M. Patriarca, and L. F. Perondi, Int. J. Modern Phys. **16**, 2823 (2002).

[37] J. Schiots, F. D. D. Tolla, and K. W. Jacobsen, Nature **391**, 561 (1998).

[38] P. Haasen, *in Physical Metallurgy, 2nd edition* (North Holland Publishing Co., R. W. Cahn (Ed.), 1970).

[39] T. Wille, G. Gieseke, and C. Schwink, Acta Mater. **35**, 2679 (1987).

[40] A. H. Cottrell, C. S. Hunter, and F. R. N. Nabarro, Philos. Mag. **44**, 1064 (1953).

[41] E. Kroner, Phys. kondens. Materie **2**, 262 (1964).

[42] R. Labush, Phys. Status Solidi **41**, 659 (1970).